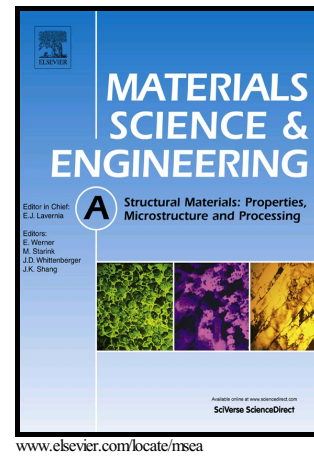


Author's Accepted Manuscript

Shape memory characteristics of a nanocrystalline TiNi alloy processed by HPT followed by post-deformation annealing

Hamed Shahmir, Mahmoud Nili-Ahmadabadi, Yi Huang, Jai Myun Jung, Hyoung Seop Kim, Terence G. Langdon



PII: S0921-5093(18)31072-4
DOI: <https://doi.org/10.1016/j.msea.2018.08.019>
Reference: MSA36790

To appear in: *Materials Science & Engineering A*

Received date: 20 June 2018
Revised date: 4 August 2018
Accepted date: 6 August 2018

Cite this article as: Hamed Shahmir, Mahmoud Nili-Ahmadabadi, Yi Huang, Jai Myun Jung, Hyoung Seop Kim and Terence G. Langdon, Shape memory characteristics of a nanocrystalline TiNi alloy processed by HPT followed by post-deformation annealing, *Materials Science & Engineering A*, <https://doi.org/10.1016/j.msea.2018.08.019>

This is a PDF file of an unedited manuscript that has been accepted for publication. As a service to our customers we are providing this early version of the manuscript. The manuscript will undergo copyediting, typesetting, and review of the resulting galley proof before it is published in its final citable form. Please note that during the production process errors may be discovered which could affect the content, and all legal disclaimers that apply to the journal pertain.

ACCEPTED MANUSCRIPT

Shape memory characteristics of a nanocrystalline TiNi alloy processed by HPT followed by post-deformation annealing

Hamed Shahmir^{a,*}, Mahmoud Nili-Ahmadabadi^a, Yi Huang^{b,c}, Jai Myun Jung^d,
Hyoung Seop Kim^d, Terence G. Langdon^b

^a *School of Metallurgy and Materials, College of Engineering, University of Tehran,
Tehran, Iran*

^b *Materials Research Group, Department of Mechanical Engineering,
University of Southampton, Southampton SO17 1BJ, UK*

^c *Department of Design and Engineering, Faculty of Science and Technology
Bournemouth University, Poole, Dorset BH12 5BB, UK*

^d *Department of Materials Science and Engineering, Pohang University of Science and
Technology, Pohang, Korea*

Abstract

A martensitic TiNi shape memory alloy was processed by high-pressure torsion (HPT) for 1.5, 10 and 20 turns followed by post-deformation annealing (PDA) at 673 and 773 K for various times in order to study the microstructural evolution during annealing and the shape memory effect (SME). Processing by HPT followed by the optimum PDA leads to an appropriate microstructure for the occurrence of a superior SME which is attributed to the strengthening of the martensitic matrix and grain refinement. A fully martensitic structure (B19' phase) with a very small grain size is ideal for the optimum SME. The results indicate that the nanocrystalline microstructures after PDA contain a martensitic B19' phase together with an R-phase and this latter phase diminishes the SME. Applying a higher annealing temperature or longer annealing time may remove the R-phase but also reduce the SME due to grain growth and the consequent decrease in the strength of the material. The results show the optimum procedure is a short-term anneal for 10 min at 673 K or only 1.5 min at 773 K after 1.5 turns of HPT processing to produce a maximum recovered strain of ~8.4% which shows more than 50% improvement compared with the solution-annealed condition.

Keywords: Crystallization; Nanostructured materials; Severe plastic deformation; Shape memory effect; TiNi alloys.

*Corresponding author. Tel.: +982182084163; fax: +982188006076

E-mail address: h.shahmir@ut.ac.ir

1. Introduction

Shape memory alloys have the ability to revert to their original shape even after severe deformation and in this respect the TiNi alloys have been widely investigated due to their superior shape memory effect (SME) amongst all shape memory alloys. The unique property of this SME is based on a thermoelastic martensitic transformation which leads to a crystallographically reversible transformation [1,2]. For the SME, plastic deformation such as slip or deformation twinning are irreversible and these strains cannot be restored even upon heating [1-4]. An increase in the critical stress by work hardening and/or grain refinement is especially important for TiNi alloys because slip is easily introduced in these alloys [5]. It is well known that grain refinement by severe plastic deformation (SPD) can improve the physical and mechanical properties of metals and alloys [6]. However, nanostructured metals and alloys processed by high-pressure torsion (HPT) exhibit limited ductility and therefore short term post-deformation annealing (PDA) at an appropriate temperature is often important to remove this limitation [7,8]. Recent studies have shown that HPT processing at relatively low temperatures may be used effectively to synthesize bulk nanostructured TiNi alloys [9-13]. It was shown also that grain refinement and the formation of a nanocrystalline microstructure suppresses the austenitic to martensitic (B19') phase transformation and promotes the formation of an intermediate martensitic phase of R in the range of ~60-150 nm [12]. The amorphization of TiNi is also significant because the grain size of specimens obtained via an amorphous state followed by crystallization due to PDA may be much smaller by comparison with those fabricated by conventional methods and this may improve their mechanical properties [13-20].

There are many reports describing the application of HPT processing to these alloys [9-21] but only very limited information is at present available on the shape memory behavior for nanocrystalline TiNi alloys prepared by HPT processing followed by PDA [22, 23]. In

principle, obtaining a fully high strength martensitic microstructure is a very important requirement for achieving good SME. It was proposed earlier that if crystallized nano-grains form after PDA then there is a critical grain size of the primary austenite for the appearance of a fully-martensitic microstructure which is ~150 nm and it was reported that HPT processing through 10 turns followed by PDA at 673 K for 60 min leads to a significantly recovered strain of ~7.8 % [22]. Very recently, it was claimed that the maximum fully recoverable strain occurs in samples with ~130 nm grain size because the local stress appearing during the martensite reorientation at room temperature is less than the yield stress for dislocation slip [23]. These two earlier investigations [22,23] confirm the importance of grain refinement during HPT followed by PDA and the formation of a fully martensitic microstructure after quenching the annealed sample to achieve the optimum SME. Nevertheless, the precise effect of the processing parameters and the role of the R-phase in SME remains unresolved.

Accordingly, and based on the limited information at present available on SME of nanocrystalline TiNi alloys, the present research was initiated to systematically investigate the effects of different numbers of rotation during HPT processing and various PDA temperatures and times on the microstructure and shape memory behavior of a representative TiNi alloy. This report focuses on the effect of grain refinement and the formation of the R-phase due to PDA as the two most important factors which appear to optimize the shape memory behavior.

2. Experimental materials and procedures

A TiNi alloy with a nominal composition of Ti-49.8at%Ni was used in these experiments: henceforth, this alloy is denoted as Ti49.8Ni. The experimental procedure was described earlier for preparing the alloy and the HPT processing [21] but briefly disks were prepared with wire electro-discharge having diameters of 10 mm and thicknesses of ~0.79-0.80 mm from a solution annealed rod processed at 1123 K for 60 minutes followed by ice-water quenching. These disks were polished and then processed at room temperature through total numbers, N , of 1.5, 10 and 20 revolutions using quasi-constrained HPT [24, 25] under an applied pressure of P

ACCEPTED MANUSCRIPT
= 2.0 GPa with a rotation speed of 0.5 rpm. The PDA was performed at 673 and 773 K in a vacuum furnace after the HPT processing for various times from 1.5 to 300 min. The heating rate of specimens in PDA was 120 K min^{-1} when measured after placing the specimens in the furnace.

Differential scanning calorimetry (DSC) analysis was performed using a DSC 200 F3 Maia® under isothermal conditions with a heating rate of 10 K min^{-1} up to 773 K. To study the phases, X-ray diffraction (XRD) was used with Cu K α radiation at 40 kV and a tube current of 30 mA. The XRD measurements were carried out over a 2θ range from 30° to 50° using a step size of 0.02° with a counting time of 9.6 s at each step. Vickers microhardness measurements were taken on surfaces polished to a mirror-like quality using a hardness tester with a load of 100 gf and dwell times of 10 s. The average microhardness values, Hv, were obtained from the average of five separate hardness values. Foil specimens for transmission electron microscopy (TEM) and high-resolution TEM (HRTEM) were prepared using electropolishing and the TEM observations were performed using a JEOL 2100 operating at 200 kV. It is important to note that circular areas of ~ 3 mm diameter were prepared for DSC, XRD, the hardness measurements and TEM from positions near the edges of the disks.

The stress-strain curves were recorded in tensile testing for a characterization of the SME using a load capacity of 2 kN and an initial strain rate of $\sim 7.4 \times 10^{-4} \text{ s}^{-1}$. The gauge dimensions of the miniature tensile specimens, which were prepared from near the edges of the HPT-processed disks by electro-discharge machining (EDM), were $2.0 \times 0.6 \times 0.5 \text{ mm}^3$. The strain recovery of the specimens was measured after loading to 8% and 10% strain followed by unloading and heating to $\sim 423 \text{ K}$ by dipping in hot oil followed by ice-water quenching. It is important to note that the samples that recovered the total strain of 8% were subjected to loading up to 10% strain.

3. Experimental results

ACCEPTED MANUSCRIPT

Figure 1 shows TEM images after HPT processing for (a) 1.5 and (b) 10 turns. Inspection shows that the specimens contain heterogeneously distributed nanocrystals marked by arrows that are embedded within an amorphous matrix but nevertheless the crystalline phases after 10 turns are clearly much smaller than after 1.5 turns. In the diffraction pattern shown in Fig. 1(a), the amorphous phase gives rise to diffuse rings superimposed with rings containing B2 (austenite) and B19' (martensite) diffraction spots of the nanocrystallites. The results indicate that, as reported elsewhere [26], the amorphous volume fraction increases with increasing degrees of deformation and hence with increasing strain.

Non-isothermal DSC measurements of the Ti49.8Ni alloy at the edges of disks are shown in Fig. 2 after solution annealing (SA: marked as $N = 0$) and after HPT processing through 1.5 to 20 turns. These non-isothermal results indicate the appearance of two exothermic peaks on the DSC thermograms after HPT processing. According to the TEM images, the microstructure of the alloy after HPT processing contains a mixture of an amorphous phase with remaining nanocrystalline austenite and martensite. Therefore, the first and second peaks are related to a crystallization of the amorphous phase and a recrystallization of the remaining crystalline phase. These results indicate, therefore, that crystallization starts at ~ 560 K and the samples are fully crystallized above ~ 660 and fully recrystallized above ~ 760 K. Based on these results, 673 and 773 K were selected as the two PDA temperatures. The integrals of the two exothermic peaks as stored energy for 1.5, 10 and 20 turns were estimated as ~ 1220 , ~ 1490 and ~ 1530 J mol⁻¹, respectively, where these results demonstrate that the microstructure does not change significantly after 10 turns.

Figure 3 shows the results of the Vickers microhardness measurements in areas very close to the edges after HPT processing through 1.5, 10 and 20 turns and PDA at (a) 673 K for 5 to 300 min and (b) 773 K for 1.5 to 10 min: the lower dashed lines denote the hardness values in the SA condition prior to HPT processing. For clarity, the individual error bars are not included

ACCEPTED MANUSCRIPT

on the datum points in Fig. 3 but the average errors on each point were typically of the order of ~2%. Inspection shows that the hardness at the edges of the disks increases significantly after only 1.5 turns such that, with reference to the SA condition, there is an overall increase by a factor of ~2.4 in the absence of PDA so that the hardness is $H_v > 450$. The torsional straining up to 20 turns leads to a very significant increase in hardness and the values after 10 and 20 turns are ~600 and ~620, respectively. After PDA, the hardness subsequently decreases with increasing annealing time due to an activation of the crystallization/recrystallization mechanisms and this decrease is significant up to 10 min at 673 K and up to 3 min at 773 K. The results also show that the hardness values after 1.5 and 10 turns of HPT reach essentially the SA value after annealing at 673 and 773 K for ~300 and ~10 min, respectively.

The X-ray diffraction patterns are shown in Fig. 4 for samples in the SA condition and after HPT processing for 20 turns followed by annealing at (a) 673 K for 0 to 120 min and (b) 773 K for 0 to 10 min. The microstructure of the SA sample is fully martensitic but the XRD patterns reveal a broadened halo-like line after 20 turns of HPT processing with a peak position corresponding to the $\{110\}_{B2(\text{austenite})}$ 2θ coordinate as reported elsewhere [13]. This confirms the austenitic phase transformation. Nevertheless, it is apparent that there are also weak extra lines close to the martensitic line positions. It is reasonable to conclude that the peak broadening with changing strain is a consequence of a structural change from a strain-induced dislocation substructure to an amorphous structure during HPT processing. However, there are peaks after PDA especially after 1.5 and 10 min annealing at 773 and 673 K, respectively. Thus, the R-phase peak appears in the XRD patterns after annealing together with the martensitic peaks after 5 min annealing and the shape and separated peaks after 10 min annealing at 673 K suggest the advent of crystallization and recrystallization. This same phenomenon also occurs after 3 min annealing at 773 K and the results show the intensity of the R-phase peak decreases with increasing annealing time.

The volume fractions of the R-phase after annealing were estimated according to a

ACCEPTED MANUSCRIPT

calculation of the R-phase volume fraction based on the XRD data [27] and the results are summarized in Table 1. Figure 5 shows that the R-phase volume fraction changes in the HPT-processed samples through different turns followed by annealing at (a) 673 and (b) 773 K for different times and this reveals the important parameters for controlling the volume fraction of the R-phase. Thus, the remaining strain in the microstructure after annealing promotes the formation of this phase and the martensitic plate size after PDA may be calculated using the well-known Scherrer equation [28] and assuming there is no strain in the material after the annealing treatment. For these calculations, the widths of the martensitic plates were calculated from the average of four separate martensitic peaks in Fig.4 and they are listed in Table 1 together with the respective annealing conditions. As anticipated, an increasing annealing time and temperature leads to the formation of larger martensitic plates. The widths of the martensitic plates in the SA condition were estimated as ~750 nm using relevant microstructural images (not shown).

The TEM images in Fig. 6 show the HPT-processed disks after (a) 1.5 and (b) 10 turns followed by isothermally annealing at a temperature of 673 K for 10 min or 30 min, respectively. It is apparent that crystallization is complete in both samples since the diffraction patterns, shown as insets, contain no diffuse rings corresponding to the amorphous phase. According to the selected area electron diffraction patterns in Fig. 6, the microstructures of specimens after annealing are martensitic together with an R-phase having an average size of the primary austenite grains (shown by arrows) of ~120 and ~140 nm for 1.5 and 10 turns, respectively. It is important to note also that the hardness of both samples is essentially the same.

Stress-strain curves were recorded for a characterization of the SME of HPT-processed samples taken through 1.5, 10 and 20 turns followed by PDA at 673 and 773 K for 10-120 min and 1.5-5 min, respectively. The strain recovery of these specimens was measured and the results are summarized in the last column of Table 1 and in Fig. 7 after loading to 8% and 10%

strain followed by unloading and heating to ~423 K by dipping in hot oil followed by ice-water quenching.

Figure 8 illustrates a typical curve for a sample after HPT processing for 1.5 turns followed by PDA at 673 K for 10 min after loading up to 10%. This curve shows a two-stage yielding behavior which can be described by the detwinning of R and B19' in the first stage and a detwinning of B19', a stress-induced R→B19' transformation and also slip in the second stage. It is important to note that the microstructure of this sample includes B19' (~71%) and R (~29%) martensitic phases based on the XRD results. It is apparent from Fig. 8 that ~3.2% of strain is recovered by unloading due to elastic and also pseudoelastic effects of the R-phase, ~5.0% of strain is recovered by heating to above the austenite finish temperature, A_f , due to SME of B19' and ~1.8% is a permanent strain due to slip and the introduction of dislocations. The result demonstrate clearly that the total recovered strain is ~8.2 which is a remarkably high value for a shape memory alloy.

Figure 9 shows representative stress-strain curves of samples after HPT followed by annealing at (a) 673 K for 30 min and (b) 773 K for only 1.5 min after loading to 8% and unloading: the arrows denote the strain recovery upon heating after unloading as represented by SME. Close inspection of these curves reveals a two-stage yielding and an increasing flow stress by increasing the rotation numbers due to HPT processing. In addition, a comparison of all curves obtained in this study (not shown) demonstrates a decreasing flow stress by increasing the annealing time. It is important to note also that the same procedure was conducted both for the SA sample and for the sample immediately after HPT processing through 1.5 turns. The results indicated that the fully-recovered strain at SA was ~5.5% upon unloading and heating whereas this value was enhanced significantly after PDA. Furthermore, the results show that, to achieve an optimum procedure with a maximum fully recovered strain of ~8.2%, it is necessary to process by HPT for only 1.5 turns followed by annealing at 673 K for 10 min or at 773 K for only 1.5 min. These results demonstrate, therefore, that the SME is

4. Discussion

4.1 Microstructures after HPT

Applying HPT processing to the martensitic TiNi yields a nanostructured phase which is produced by deformation-induced grain fragmentation and concomitant amorphization. It has been proposed that lattice dislocations may cause localized amorphization through an accumulation of the martensitic substructure within the initial grains at grain boundaries and twin boundaries [11,12]. In addition, it appears that the amorphous phase induced by HPT-processing can occur in shear bands as shown by the dashed lines in Fig. 1 and also as reported elsewhere [26]. The appearance of B2 diffraction spots, consistent with the XRD results in Fig. 4, indicates the occurrence of a reverse transformation from martensite to austenite induced by the severe plastic deformation. It has been reported that most of the nanocrystallites contain austenite whereas prior to HPT the crystalline structure is fully martensitic [14].

A major challenge in using HPT processing is that it introduces a significant inhomogeneity in the material because the strain varies throughout the disk [29,30]. In practice, however, the nonuniformity of stress and hardness, as well as the inhomogeneity of the dislocation density, becomes weaker with progressive straining because the dislocation density tends to saturate at large strains [31]. For the TiNi alloy, based on earlier investigations of the same alloy using HPT-processing, the results indicate that HPT produces a martensite-to-austenite and then a crystal-to-amorphous phase transformation with increasing numbers of rotations [21,22]. These phenomena are associated with an intensive ($N = 1.5$) and then a gradual ($N > 1.5$) increase in hardness across the disk diameters and the presence of an almost homogeneous hardness distribution and saturation hardness at $H_v \approx 620$ after 10 turns. However, it was reported that there was no fully homogeneous hardness distribution even after 20 turns and the area within a radius of $r \approx 200 \mu\text{m}$ at the center of the disk continued to have a lower hardness [21]. These results demonstrate, therefore, that the microstructure does not

change significantly after 10 turns and this was further confirmed by the stored energy values estimated from the DSC results (~ 1490 and 1530 J mol^{-1} for HPT-processed samples through 10 and 20 turns, respectively). The TEM image and DSC results clearly represent a dual phase and the existence of an inhomogeneity in the microstructure after HPT processing.

4.2 Annealing behavior

The results in the present investigation indicate that, even after 10 turns of HPT, the microstructure is not fully amorphous and debris, in the form of nanocrystals and heterogeneities of crystal-like medium-range order, are embedded in the amorphous where they can act as nucleation sites due to heat activated phenomena such as a crystallization of the amorphous phase. This inhomogeneity in the microstructure may be responsible for a further inhomogeneity in the microstructure of samples after subjecting to PDA. Close inspection of the TEM images after PDA (Fig 6) confirms this inhomogeneity through the formation of a range of grain sizes in the microstructures from ~ 30 to ~ 130 nm. This non-isothermal analysis suggests that crystallization and recrystallization start at 563 and 658 K, respectively. A previous investigation on the effect of various SPD procedures, such as equal-channel angular pressing, repetitive corrugation and straightening by rolling and heavy cold rolling, on the martensitic TiNi alloy show there is a significant martensitic stabilization after SPD and thermal analyses further indicate that the recovery and recrystallization temperature is of the order of ~ 673 K [32]. Therefore, no amorphous phase is expected after annealing at >673 K, and this is fully supported by the consequent significant drops in hardness (Fig. 3) and the formation of sharp peaks in the XRD patterns (Fig. 4) after annealing at 673 K for 10 min and also after annealing at 773 K for only 1.5 min.

In addition, the present results indicate that 5 min is not a sufficient annealing time to effectively reverse the amorphous-to- crystal phase transformation activated by heating at 673 K. Thus, the results show that the microstructure after PDA and ice-water quenching is martensitic together with an R-phase. Close inspection of the XRD patterns of samples after

ACCEPTED MANUSCRIPT
short-term annealing reveals that the R-phase is the main phase in the sample annealed for 1.5 min at 773 K (Fig. 5) and there is even an austenitic phase together with an R-phase in the sample annealed for 5 min at 673 K.

Concerning the appearance of the austenite and R phase in the microstructure after annealing, it was reported that the martensitic transformation is suppressed with a decrease in grain size so that the austenitic phase is stable at grain sizes lower than ~60 nm and the R-phase appears in the range of ~60-150 nm [12]. The present results demonstrate that the grain size of the primary austenite in the samples after 1.5 turns of HPT followed by PDA at 673 K for 10 min and after 10 turns of HPT followed by PDA at 673 K for 30 min after annealing at 673 K are ~120-140 nm, and this is within the range of ~60-150 nm so that the appearance of the R-phase in the diffraction pattern and the corresponding XRD results are reasonable. The data presented in Table 1 show clearly the effect of straining during HPT and the role of annealing time and temperature to control the volume fraction of the R-phase.

It is important to note that nanocrystallization occurs at an annealing temperature as low as 673 K since the retained crystallites act as heterogeneous nucleation sites giving a high nucleation rate although the growth rate is low because this temperature is far below $0.5T_m$ (~850 K) where T_m is the absolute melting temperature. As expected from kinetic considerations, crystallization/recrystallization at a temperature such as 773 K is extremely fast and this produces intensive changes after very short annealing times of only 1.5 min. Therefore, annealing at 773 K for more than 1.5 min in all HPT-processed samples leads to an intensive coarsening. Finally, it is important to note that, according to the heating rate of the furnace (~120 K min⁻¹), this temperature is reached after only ~4 min.

4.3 Improving the shape memory effect

In principle, a fully martensitic microstructure with appropriate strength plays an important role in attaining the optimum SME. The martensitic reorientation when one martensite variant

grows due to other variants shrinking during loading is the main mechanism for deformation of the TiNi alloy in the martensitic state. This process may result in a high stress appearing in local sites on the interfaces between variants and on the grain interfaces, and this local stress may exceed the yield stress for dislocation slip so that it is accompanied by plastic deformation [1,2]. The strain appearing during the martensitic reorientation is recoverable whereas the plastic strain is not recoverable. Therefore, a poor SME (~5.5 recovery strain) of the SA specimen in the present study was predicted by comparison with specimens after PDA due to the relatively low strength of the material in this condition. This confirms that an increase of the critical stress by grain refinement produces a significant improvement in the SME.

The present analysis explains the poor SME of the samples after either a long term annealing (120 min at 673 K) or an annealing at higher temperatures (773 K for 5 min) due to a consequent decrease in the strength of the materials as shown by the microhardness results in Fig. 3 and Table 1 by comparison with other annealing conditions. Therefore, increasing the grain size produces a decrease in the yield stress for dislocation slip which is more effective than the local stress and thereby provides a condition for an increase in the permanent strain.

The results show clearly that the severely deformed specimens and the specimens with very small grain sizes (as in samples processed by HPT through 10 and 20 turns followed by PDA at 773 K for only 1.5 min) exhibit poor SMEs (~5.3 % recovery strain for a sample processed by HPT through 1.5 turns). In the case of severely deformed samples, it was proposed that the recovery strain decreases by increasing the strain and there is a saturation of strain hardening in the TiNi alloys [2]. Since the specimen contains an amorphous phase after severe plastic deformation, it is expected that specimens after 1.5 turns of HPT will exhibit a poor SME. In addition, it was claimed that the reorientation of the martensite in nanograins and the formation of a single variant during active deformation should be partially or fully suppressed in very small grains of the TiNi alloys where this can significantly affect the shape memory behavior and diminish the recoverable strain [2].

ACCEPTED MANUSCRIPT

The present results prove clearly the existence of an R-phase (or even an austenitic phase) in the microstructures after PDA under different conditions (Fig. 4) and this plays an important role in the shape memory behavior of the specimens. It is important to note that the R-phase shows pseudoelasticity due to the R→B19' transformation and the SME but the available pseudoelasticity and shape memory strain is very small (~1%) and this is significantly lower than for the B19' phase. Therefore, it is expected that the existence of the R-phase in the microstructure produces a reduction in the SME [33,34]. A clear two-stage yielding is observed during loading up to 10% in Fig. 8 which shows the pseudoelasticity associated with the R-phase transition upon unloading and also strain recovery upon heating to temperatures above A_f . These two-stage yieldings were observed earlier in the fully R-phase samples which were related to the rearrangement of the R-phase variants and the following R→B19' martensitic transformation [34]. It was reported earlier for this alloy that severe plastic deformation by differential speed rolling with high speed followed by PDA at 673 K led to a deterioration in the shape memory properties which was attributed to the formation of the R-phase and an increase of the martensitic finish temperature, M_f [35].

Close inspection of Fig. 9(b) and Fig. 5(b) reveals the effect of the R-phase volume fraction on the amount of the recovered strain by unloading in the pseudoelastic effect. Thus, a high value of the R phase promotes the pseudoelastic behaviour but diminishes the total recovered strain. Concerning the origin of the R-phase in nanostructured TiNi alloys produced by HPT followed by PDA, it was reported that for grains in the range of ~60-150 nm the R-phase appears in dislocation-free nanograins [12] which is consistent with the present results. These results also demonstrate that achieving a homogenous microstructure with a primary austenitic grain size of ~150 nm is not possible due to the intrinsic inhomogeneity of the HPT-processed sample. The TEM images in Fig. 1 and the DSC results in Fig. 2 show clearly this inhomogeneity after HPT processing. Therefore, the microstructure after PDA is not homogenous as is evident from Fig. 6 and it includes both finer and larger grains formed in the

amorphous and crystalline areas, respectively. Accordingly, the formation of the R-phase in the finer grain sizes is predictable. It is important to note also that applying higher and longer annealing temperatures and/or times to prepare a homogenous microstructure, or at least to increase the grain size of the finer grain to sizes larger than the range of ~60-150 nm, leads to a decrease in the strength and hence a deterioration in the SME.

These results indicate that the recovered strain for the nanocrystalline microstructure, obtained after annealing at 673 K for short times up to 30 min, is not as satisfactory as for the 60 min condition because of the existence of a high volume fraction of the R-phase. Thus, a good SME is not expected after annealing for 5 min at 673 K because the R-phase is dominant and/or the crystallization has not finished.

Finally, it is concluded that SPD processing followed by the optimum PDA leads to an appropriate microstructure with an optimum grain size of primary austenite which is both not too small to suppress and promote the formation of the B19' and R-phases, respectively, and not too large to prevent grain growth and thereby provide a high strength of martensite. This optimum amount of the R-phase then leads directly to the occurrence of a superior SME. The results show also that it is not possible to completely remove the R-phase completely using the present annealing conditions as in Fig. 5 and higher annealing temperatures and longer annealing times will produce a deterioration in the SME due to grain growth and a consequent decrease in the strength of the material. Nevertheless, short-term annealing at 673 K for 10 min or at 773 K for 1.5 min after only 1.5 turns of HPT processing is clearly the most favorable procedure for obtaining an outstanding shape memory behavior due to the dual benefits of grain refinement and an effective control of the amount of the R-phase. This procedure provides a maximum recovered strain of up to ~8.4% with an improvement compared with the SA condition of more than 50%.

5. Summary and conclusions

1. Applying HPT processing to a martensitic Ti-49.8at%Ti alloy yields a nanostructured

ACCEPTED MANUSCRIPT
phase and concomitant amorphization. The results show an amorphization transformation when the rotational straining is continued to an acceptable level of homogeneity in hardness and to almost saturation after 10 turns of HPT processing.

2. Crystallization of the amorphous phase and recrystallization of the crystalline phase occur after post-deformation annealing at 673 and 773 K. The results indicate that the nanocrystalline microstructure after PDA and ice-water quenching is martensitic together with an R-phase.

3. These results suggest that a refined grain size and the existence of an R-phase are two important factors contributing to a superior SME. High annealing temperatures and long annealing times may remove the R-phase but with a consequent deterioration in the SME due to grain growth and a decrease in the strength of the material.

4. A short-term anneal for 10 min at 673 K or only 1.5 min at 773 K after 1.5 turns of HPT appears to be the optimum procedure with a maximum recovered strain of up to ~8.4% and an improvement of more than 50% by comparison with the SA condition.

Acknowledgements

This work was supported by the National Elites Foundation of the Islamic Republic of Iran and in part by the European Research Council under Grant Agreement No. 267464-SPDMETALS (TGL). In addition, the work was supported by the National Research Foundation of Korea (NRF) grant funded by the Korea government (MSIP) (No. 2014R1A2A1A10051322).

1. K. Otsuka, C.M. Wayman (eds), Shape Memory Materials, Cambridge University Press, Cambridge, U.K. (1999).
2. K. Otsuka, X. Ren, Physical metallurgy of Ti–Ni-based shape memory alloys, *Prog. Mater. Sci.* 50 (2005) 511-678.
3. D. Wurzel, Marforming and tempering of binary Ni-Ti alloys including precipitation effects, *Mater. Sci. Eng. A* 273-275 (1999) 634-638.
4. E. Hornbogen, V. Mertinger, D. Wurzel, Microstructure and tensile properties of two binary NiTi-alloys, *Scr. Mater.* 44 (2001) 171-178.
5. S. Miyazaki, Y. Ohmi, K. Otsuka, Y. Suzuki, Characteristics of deformation and transformation pseudoelasticity in Ti–Ni alloys, *J. Phys.* 43 (C4) (1982) 255-260.
6. T.G. Langdon, Twenty-five years of ultrafine-grained materials: Achieving exceptional properties through grain refinement, *Acta Mater.* 61 (2013) 7035-7059.
7. R.Z. Valiev, A.V. Sergueeva, A.K. Mukherjee, The effect of annealing on tensile deformation behaviour of nanostructured SPD titanium, *Scr. Mater.* 49 (2003) 669-674.
8. Y. Huang, M. Lemang, N.X. Zhang, P.H.R. Pereira, T.G. Langdon, Achieving superior grain refinement and mechanical properties in vanadium through high-pressure torsion and subsequent short-term annealing, *Mater. Sci. Eng. A* 655 (2016) 60-69.
9. V.G. Pushin, V.V. Stolyarov, R.Z. Valiev, T.C. Lowe, Y.T. Zhu, Nanostructured TiNi-based shape memory alloys processed by severe plastic deformation, *Mater. Sci. Eng. A* 410 (2005) 386-389.
10. A.V. Sergueeva, C. Song, R.Z. Valiev, A.K. Mukherjee, Structure and properties of amorphous and nanocrystalline NiTi prepared by severe plastic deformation and annealing, *Mater. Sci. Eng. A* 339 (2003) 159-165.
11. T. Waitz, H.P. Karnthaler, Martensitic transformation of NiTi nanocrystals embedded in an amorphous matrix, *Acta Mater.* 52 (2004) 5461-5469.

12. T. Waitz, V. Kazykhanov, H.P. Karnthaler, Martensitic phase transformations in nanocrystalline NiTi studied by TEM, *Acta Mater.* 52 (2004) 137-147.
13. S.D. Prokoshkin, I.Y. Khmelevskaya, S.V. Dobatkin, I.B. Trubitsyna, E.V. Tatyatin, V.V. Stolyarov, E.A. Prokofiev, Alloy composition, deformation temperature, pressure and post-deformation annealing effects in severely deformed Ti–Ni based shape memory alloys, *Acta Mater.* 53 (2005) 2703-2714.
14. C. Rentenberger, T. Waitz, H.P. Karnthaler, Formation and structures of bulk nanocrystalline intermetallic alloys studied by transmission electron microscopy, *Mater.Sci. Eng. A* 462 (2007) 283-288.
15. M. Peterlechner, T. Waitz, H.P. Karnthaler, Nanocrystallization of NiTi shape memory alloys made amorphous by high-pressure torsion, *Scr. Mater.* 59 (2008) 566-569.
16. M. Peterlechner, T. Waitz, H.P. Karnthaler, Nanoscale amorphization of severely deformed NiTi shape memory alloys, *Scr. Mater.* 60 (2009) 1137-1140.
17. I.Y. Khmelevskaya, S.D. Prokoshkin, S.V. Dobatkin, E.V. Tatyatin, I.B. Trubitsyna, Studies of composition, deformation temperature and pressure effects on structure formation in severely deformed TiNi-based alloys, *Mater. Sci. Eng. A* 438-440 (2006) 472-475.
18. R. Z. Valiev, D. V. Gunderov, A. V. Lukyanov, V. G. Pushin, Mechanical behavior of nanocrystalline TiNi alloy produced by severe plastic deformation, *J. Mater. Sci.* 47, 2012, 7848-7853.
19. R. Singh, H. Rosner, E.A. Prokofyev, R.Z. Valiev, S.V. Divinski, G. Wilde, Annealing behaviour of nanocrystalline NiTi (50 at% Ni) alloy produced by high-pressure torsion, *Phil. Mag.* 91 (2011) 3079-3092.
20. N. Resnina, S. Belyaev, V. Zeldovich, V. Pilyugin, N. Frolova, D. Glazova, Variations in martensitic transformation parameters due to grain evolution during post-deformation heating of Ti-50.2 at.% Ni alloy amorphized by HPT, *Thermochimica Acta* 627-629 (2016)

21. H. Shahmir, M. Nili-Ahmadabadi, Y. Huang, T.G. Langdon, Evolution of microstructure and hardness in NiTi shape memory alloys processed by high-pressure torsion, *J. Mater. Sci.* 49 (2014) 2998-3009.
22. H. Shahmir, M. Nili-Ahmadabadi, Y. Huang, J.M. Jung, H.S. Kim, T.G. Langdon, Shape memory effect in nanocrystalline NiTi alloy processed by high-pressure torsion, *J. Mater. Sci. Eng. A* 626 (2015) 203-206.
23. S. Belyaev, N. Resnina, V. Pilyugin, D. Glazova, V. Zeldovich, N. Frolova, Shape memory effects in Ti-50.2 at% Ni alloy with different grain size, *J. Mater. Sci. Eng. A* 706 (2017) 64-70.
24. R.B. Figueiredo, P.R. Cetlin, T.G. Langdon, Using finite element modeling to examine the flow processes in quasi-constrained high-pressure torsion, *J. Mater. Sci. Eng. A* 528 (2011) 8198-8204.
25. R.B. Figueiredo, P.H.R. Pereira, M.T.P. Aguilar, P.R. Cetlin, T.G. Langdon, Using finite element modeling to examine the temperature distribution in quasi-constrained high-pressure torsion, *Acta Mater.* 60 (2012) 3190-3198.
26. M. Peterlechner, J. Bokeloh, G. Wilde, T. Waitz, Study of relaxation and crystallization kinetics of NiTi made amorphous by repeated cold rolling, *Acta Mater.* 58 (2010) 6637-6648.
27. B.D. Cullity, S.R. Stock, *Elements of X-ray Diffraction*, 3rd Ed, Englewood Cliffs, Prentice Hall, NJ, U.S.A. (2001).
28. A.L. Patterson, The Scherrer formula for X-Ray particle size determination, *Phys. Rev.* 56 (1939) 978-982.
29. A.P. Zhilyaev, T.G. Langdon, Using high-pressure torsion for metal processing: Fundamentals and applications, *Prog. Mater. Sci.* 53 (2008) 893-979.
30. S.C. Yoon, Z. Horita, H.S. Kim, Finite element analysis of plastic deformation behavior

31. H.W. Park, L.J. Park, Y. Estrin, H.S. Kim, Dislocation density-based finite element analysis of large strain deformation behavior of copper under high-pressure torsion, *Acta Mater.* 76 (2014) 281-293.
32. H. Shahmir, M. Nili-Ahmadabadi, A. Razzaghi, M. Mohammadi, C.T. Wang, J.M. Jung, H.S. Kim, T.G. Langdon, Using dilatometry to study martensitic stabilization and recrystallization kinetics in a severely deformed TiNi alloy, *J. Mater. Sci.* 50 (2015) 4003-4011.
33. S. Miyazaki, S. Kimura, K. Otsuka, Shape-memory effect and pseudoelasticity associated with the R-phase transition in Ti-50.5 % Ni single crystals, *Philos. Mag.* A57 (1988) 467-478.
34. S. Miyazaki, K. Otsuka, Deformation and transition behavior associated with the R-phase in Ti-Ni alloys, *Metall Trans* 17A (1986) 53-63.
35. Y.G. Lim, S.H. Han, E.S. Choi, W.J. Kim, Enhancement of recovery stresses of the Ni-50.2Ti alloy by severe plastic deformation using a high-ratio differential speed rolling technique, *Scr. Mater.* 124 (2016) 95-98.

Table 1. The Vickers microhardness, martensite plate size, volume fraction of R-phase and recovered strain of stress–strain curves after loading up to 8% (and 10% for some conditions) and unloading followed by heating to ~423 K.

Figures captions

Fig. 1 TEM images and corresponding diffraction patterns of the Ti49.8Ni after (a) 1.5 turns and (b) 10 turns of HPT processing; the severely deformed microstructure contains amorphous and nano-size fragments (marked by arrows) and the corresponding diffraction pattern shows the arrangements of the diffraction spots in semi-continuous circles related to B2 and B19' phases in the microstructure. Shear band also indicated by dashed lines.

Fig. 2 Non-Isothermal (scanning) DSC measurement of Ti49.8Ni after solution annealing and HPT processing: the heating rate is 10 K min⁻¹.

Fig. 3 Microhardness distribution along the radius of the Ti49.8Ni disks after HPT processing and PDA at (a) 673 K and (b) 773 K for various times.

Fig. 4 X-ray patterns of Ti49.8Ni after 20 turns HPT processing and PDA at (a) 673 K and (b) 773 K for various times.

Fig. 5 Volume fraction of R-phase in Ti49.8Ni after HPT processing through 1.5, 10 and 20 turns followed by PDA at (a) 673 K and (b) 773 K for various times, estimated from XRD results.

Fig. 6 TEM images and corresponding diffraction patterns of nanocrystalline Ti49.8Ni alloy (a) after 1.5 turns of HPT followed by PDA at 673 K for 10 min and (b) after 10 turns of HPT followed by PDA at 673 K for 30 min: the average sizes of the primary austenite grains (shown

by arrows) are ~120 and 140 nm, respectively.

Fig. 7 Recovered strain of HPT samples after PDA at 673 and 873 K for various times: these value obtained after loading followed by heating after unloading.

Fig. 8 Stress–strain curves of Ti49.8Ni after HPT processing for 1.5 turns followed by PDA at 673 K for 10 min after loading up to 10%; the total recovered strain and permanent strain are ~8.2 and 1.8 %, respectively.

Fig. 9 Stress–strain curves of Ti49.8Ni after HPT processing for 1.5, 10 and 20 turns followed by PDA at (a) 673 K for 30 min and (b) 773 K for 1.5 min: the arrows show the strain recovery upon heating after unloading.

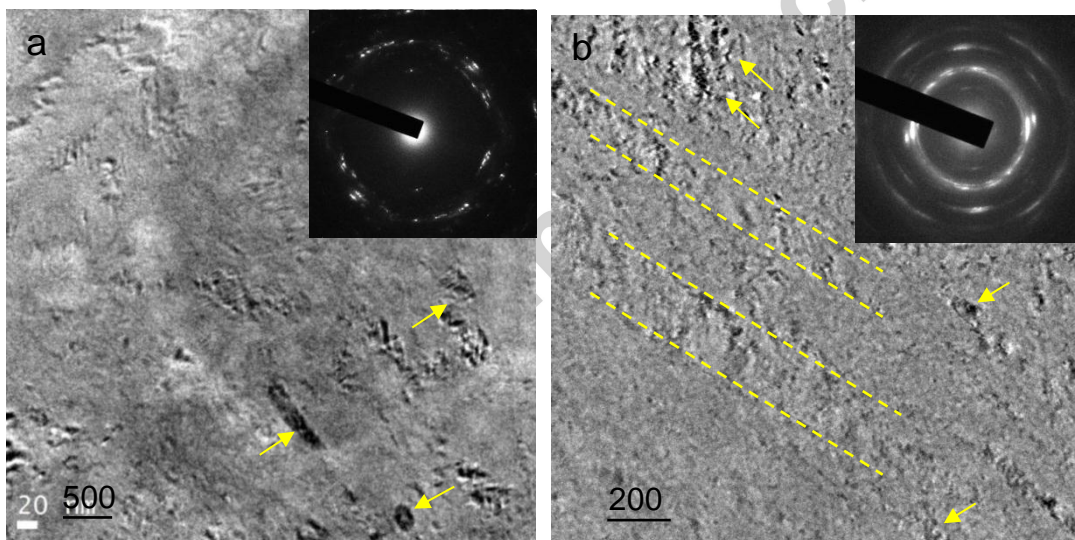


Fig. 1 TEM images and corresponding diffraction patterns of the Ti49.8Ni after (a) 1.5 turns and (b) 10 turns of HPT processing; the severely deformed microstructure contains amorphous and nano-size fragments (marked by arrows) and the corresponding diffraction pattern shows

phases in the microstructure. Shear band also indicated by dashed lines.

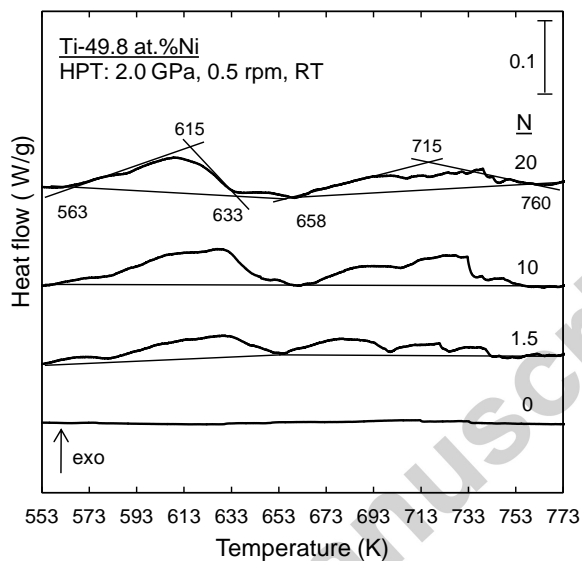
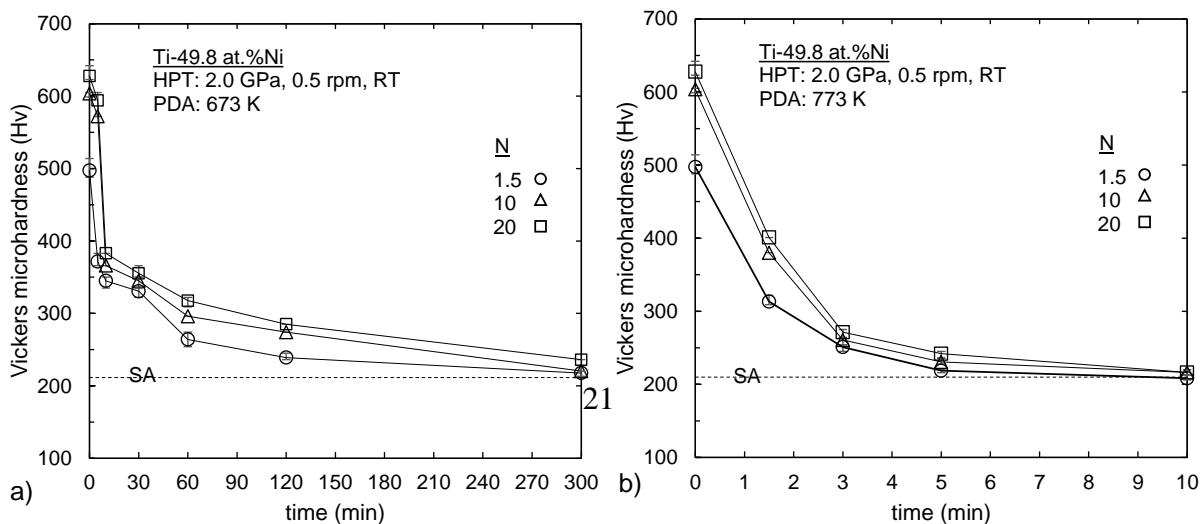


Fig. 2 Non-Isothermal (scanning) DSC measurement of Ti49.8Ni after solution annealing and HPT processing: the heating rate is 10 K min⁻¹.



Accepted manuscript

Fig. 3 Microhardness distribution along the radius of the Ti49.8Ni disks after HPT processing and PDA at (a) 673 K and (b) 773 K for various times.

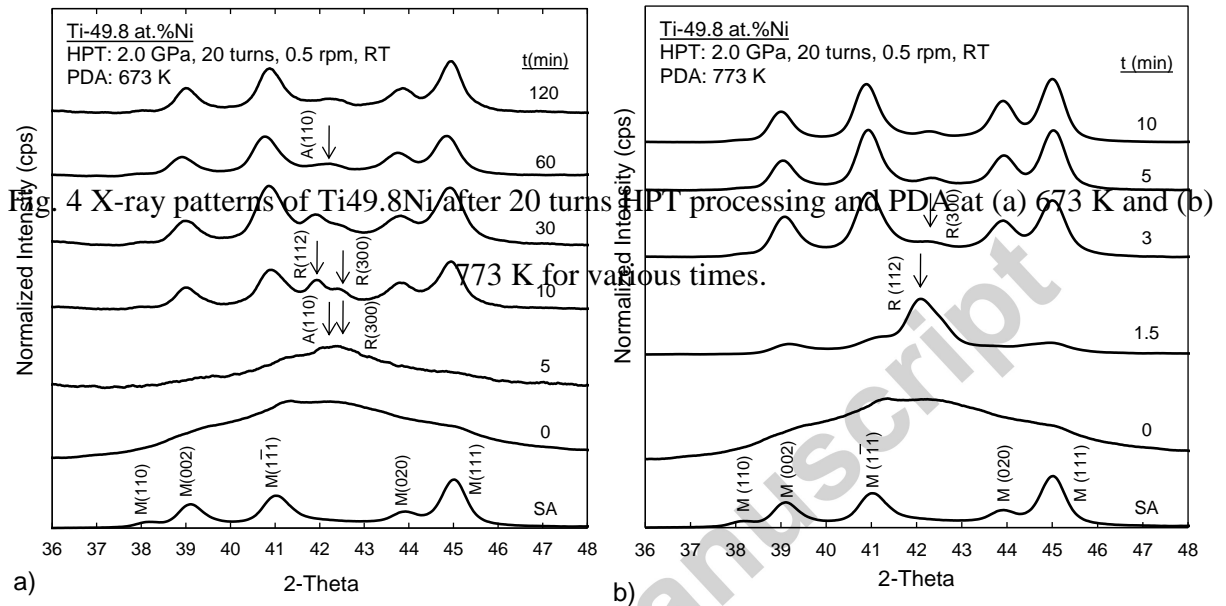


Fig. 4 X-ray patterns of Ti49.8Ni after 20 turns HPT processing and PDA at (a) 673 K and (b) 773 K for various times.

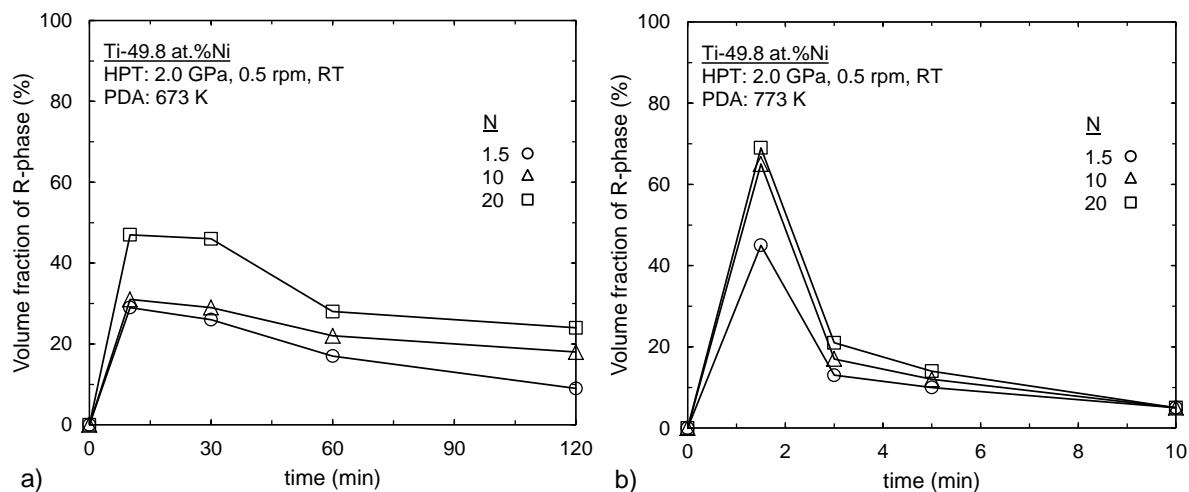
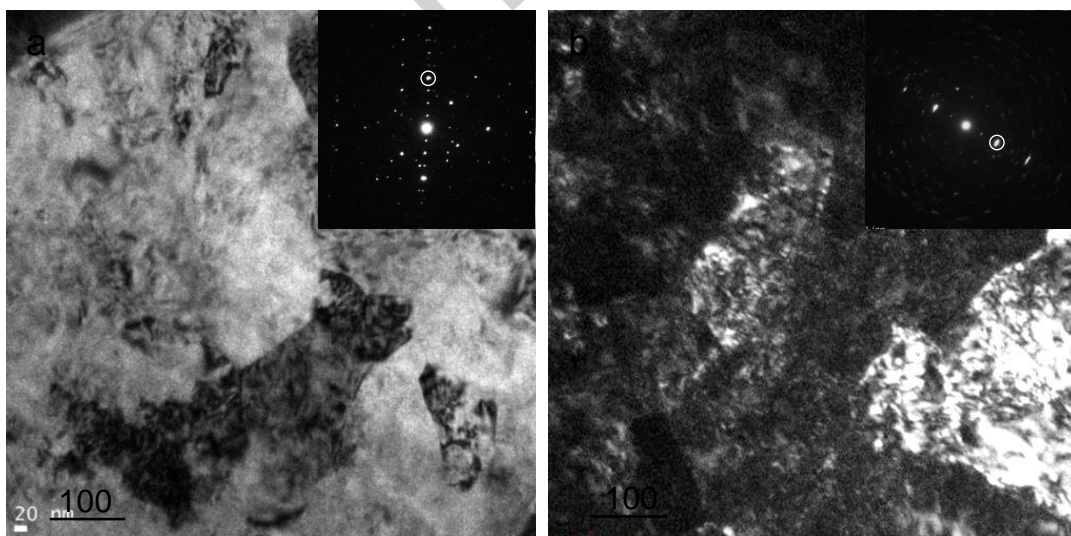


Fig. 5 Volume fraction of R-phase in Ti49.8Ni after HPT processing trough 1.5, 10 and 20 turns followed by PDA at (a) 673 K and (b) 773 K for various times, estimated from XRD results.



ACCEPTED MANUSCRIPT

Fig. 6 TEM images and corresponding diffraction patterns of nanocrystalline Ti_{49.8}Ni alloy (a) after 1.5 turns of HPT followed by PDA at 673 K for 10 min and (b) after 10 turns of HPT followed by PDA at 673 K for 30 min: the average size of the primary austenite grains (shown by arrows) are ~120 and 140 nm, respectively.

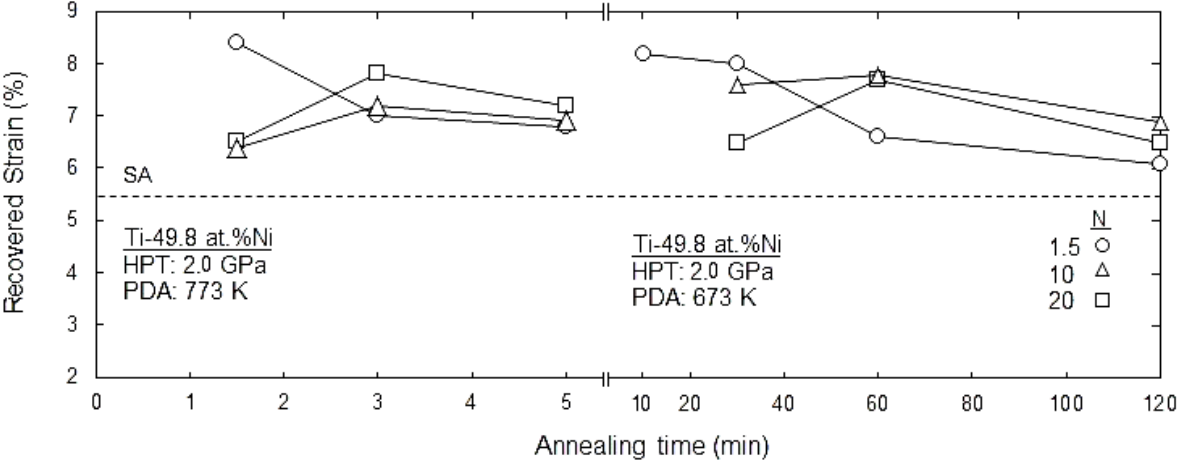


Fig. 7 Recovered strain of HPT samples after PDA at 673 and 873 K for various time: these value obtained after loading followed by heating after unloading.

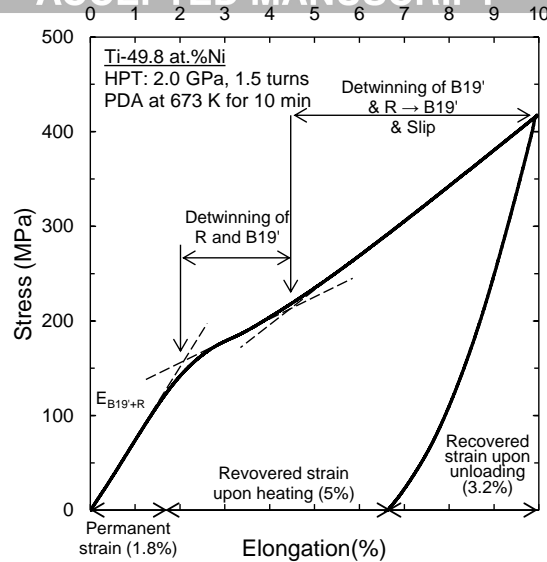


Fig. 8 Stress–strain curves of Ti49.8Ni after HPT processing for 1.5 turns followed by PDA at 673 K for 10 min after loading up to 10%; the total recovered strain and permanent strain are 8.2 and 1.8 %, respectively.

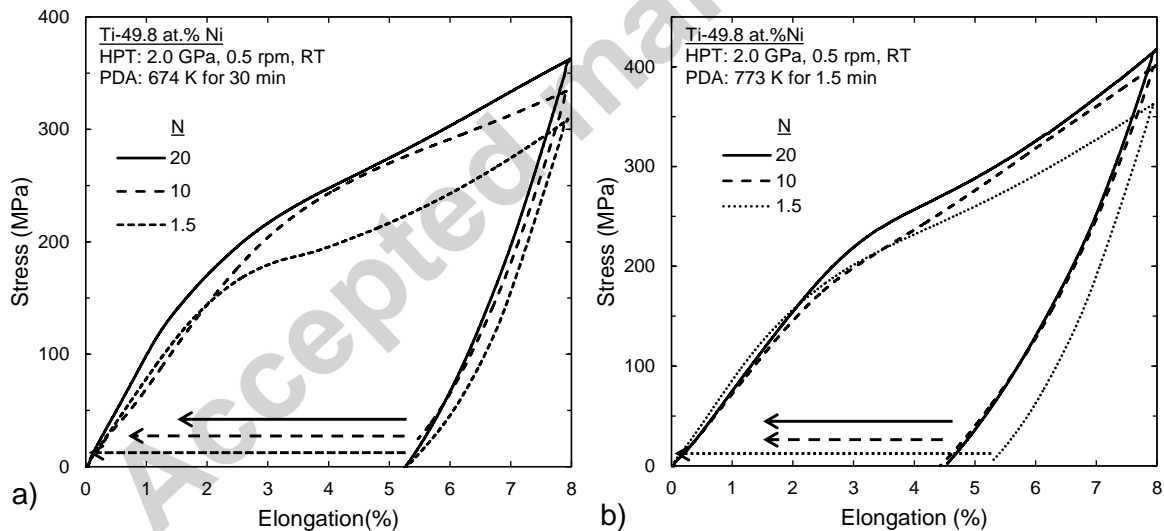


Fig. 9 Stress–strain curves of Ti49.8Ni after HPT processing for 1.5, 10 and 20 turns followed by PDA at (a) 673 K for 30 min and (b) 773 K for 1.5 min: the arrows show the strain recovery upon heating after unloading.

Table 1. The Vickers microhardness, martensite plate size, volume fraction of R-phase and recovered strain of stress–strain curves after loading up to 8% (and 10% for some conditions) and unloading followed by heating to ~423 K.

Number of rotations	Annealing temp. (K)	Annealing time (min)	Hv	Martensite plate size (nm)	R phase (%)	Total recovered strain (%)
0 (SA)	-	-	210±4	750±250	0	5.5
1.5	-	0	497±12	12±2	0	5.3
	673	10	340±7	35±7	29	8*
	673	30	330±6	38±8	26	8.2*
	673	60	264±10	111±26	17	6.6
	773	1.5	336±6	20±2	42	8.4*
	773	3	251±4	105±15	13	7
	773	5	218±2	>200	10	7
10	673	10	366±6	22±4	31	-
	673	30	340±7	40±2	29	7.6
	673	60	304±2	55±3	22	7.8
	673	120	274±2	>200	18	6.9
	773	1.5	380±2	26±6	61	6.4
	773	3	260±3	122±24	17	7.2
	773	5	231±3	>200	12	7.0
20	673	10	377±8	23±7	47	-
	673	30	355±7	30±6	46	6.5
	673	60	318±7	47±8	28	7.7
	673	120	266±5	>200	24	6.5
	773	1.5	401±2	18±3	64	6.5
	773	3	271±3	>200	21	7.8
	773	5	242±3	>200	14	7.2

* The samples that recovered the total strain of 8% were subjected to loading up to 10% strain.